The Astrophysical Journal, 660:1039–1050, 2007 May 10

THE NUCLEAR TO HOST GALAXY RELATION OF HIGH-REDSHIFT QUASARS

Jari K. Kotilainen
Tuorla Observatory, University of Turku, Väisäläntie 20, FI-21500 Piikkiö, Finland; jarkot@utu.fi

Renato Falomo
INAF-Osservatorio Astronomico di Padova, Vicolo dell'Osservatorio 5, 35122 Padova, Italy; falomo@pd.astro.it

Marzia Labita and Aldo Treves
Università dell'Insubria, via Valleggio 11, I-22100 Como, Italy; marzia.labita@uninsubria.it, treves@mib.infn.it

and

Michela Uslenghi
INAF-IASF Milano, Via E. Bassini 15, Milano I-20133, Italy; uslenghi@iasf-milano.inaf.it
Received 2006 July 15; accepted 2007 January 14

ABSTRACT

We present near-infrared imaging of the host galaxies of low-luminosity quasars at $1 < z < 2$, aimed at investigating the relationship between the nuclear and host-galaxy luminosities at high redshift. This work complements our previous study to trace the cosmological evolution of the host galaxies of high-luminosity quasars. The sample consists of nine radio-loud (RLQ) and six radio-quiet (RQQ) low-luminosity quasars. They have similar redshift and optical luminosity distributions, and together with the high-luminosity quasars, cover a large range of the quasar luminosity function. For all but two of the quasars, we have been able to derive the global properties of the surrounding nebulosity. The host galaxies of both types of quasars are massive inactive ellipticals between L^* and $10L^*$, with RLQ hosts being significantly more luminous than RQQ hosts. This luminosity gap is independent of the rest-frame *U*-band luminosity but correlated with the rest-frame *R*-band luminosity. The color difference between the RQQs and the RLQs is likely a combination of an intrinsic difference in the strength of the thermal and nonthermal components in their SEDs, and a selection effect due to internal dust extinction. For the combined set of quasars, we find a reasonable correlation between the nuclear and the host luminosities. This correlation is less apparent for RQQs than for RLQs. If the *R*-band luminosity represents the bolometric luminosity, and the host luminosity is proportional to the black hole mass, as in nearby massive spheroids, quasars emit in a relatively narrow range with respect to their Eddington luminosity and with the same distribution for RLQs and RQQs.

Subject headings: galaxies: active — galaxies: evolution — infrared: galaxies — quasars: general

Online material: color figure

1. INTRODUCTION

Low-redshift ($z \leq 0.5$) quasars are predominantly hosted by luminous, massive, bulge-dominated galaxies (e.g., McLeod & Rieke 1994; Taylor et al. 1996; Bahcall et al. 1997; Percival et al. 2001; Hamilton et al. 2002; Dunlop et al. 2003; Pagani et al. 2003; Floyd et al. 2004). More specifically, the nature of the host depends on nuclear luminosity, in the sense that high-luminosity quasars are exclusively hosted in elliptical galaxies, while fainter radio-quiet quasars can also be found in early-type spirals (Hamilton et al. 2002; Dunlop et al. 2003). This trend is consistent with the fact that low-luminosity type 1 AGNs (e.g., Seyfert 1 galaxies) are only found in spiral galaxies (e.g., Kotilainen & Ward 1994; Hunt et al. 1997).

This scenario is consistent with the fact that practically all nearby massive spheroids (ellipticals and bulges of early-type spirals) have an inactive supermassive black hole (BH) in their centers (see e.g., Barth 2004; Ferrarese 2006 for recent reviews) and that more massive bulges host the most massive BHs. This suggests that episodic quasar activity (with a varying duty cycle) may be very common in massive galaxies and that the nuclear power depends on the mass of the galaxy. Powerful quasar activity is in fact only found in the most luminous (massive) galaxies (Hamilton et al. 2002; Falomo et al. 2003; Kauffmann et al. 2003). At low redshift, the mass of the BH is correlated to the luminosity and the velocity dispersion of the bulge (e.g., Magorrian et al. 1998; Ferrarese & Merritt 2000; Gebhardt et al. 2000; McLure & Dunlop 2002; Marconi & Hunt 2003; Bettoni et al. 2003; Häring & Rix 2004). Furthermore, the strong cosmological evolution of the quasar population, with a comoving space density peak at $z \sim 2$–3 before rapidly declining to its low present value (Dunlop & Peacock 1990; Warren et al. 1994; Boyle 2001), is similar to the BH mass accretion rate and the evolution of the cosmic star formation history (Madau et al. 1998; Franceschini et al. 1999; Steidel et al. 1999; Chary & Elbaz 2001; Barger et al. 2001; Yu & Tremaine 2002; Marconi et al. 2004). Therefore, determining how the properties of the galaxies hosting quasars evolve with the cosmic time may be crucial to investigating the fundamental link between the formation and evolution of massive galaxy bulges and their nuclear activity, and to reveal whether BHs and spheroids really grow synchronously.

The detection of the host galaxies for high-redshift objects and the characterization of their properties is rather challenging because the host galaxy rapidly becomes very faint compared to the nucleus. In order to cope with this, imaging with high spatial resolution and S/N, together with a well-defined point-spread function (PSF) for modeling the images are of crucial importance.

In a previous work (Falomo et al. 2004) with the 8 m Very Large Telescope (VLT) and ISAAC, we have carried out a systematic imaging study, under excellent seeing conditions (median

TABLE 1
Journal of Observations

Quasar	z	V[a]	Date	Filter	t_{exp}[b] (minutes)	Seeing[c] (arcsec)	Number[d]
Radio-Quiet Quasars							
Q0335−3546	1.841	19.8	2004 Nov 01	*K*	36	0.34	4
MS 0824.2+0327	1.431	20.2	2004 Dec 24	*K*	36	0.33	5
2QZ J101733−0049	1.342	20.4	2004 Dec 25	*H*	36	0.47	4
2QZ J101733−0203	1.895[e]	20.8	2004 Dec 26	*K*	36	0.32	6
TOL 1033.1−27.3	1.610	21.8	2004 Dec 26	*K*	36	0.32	4
Q1045+056	1.230	20.3	2005 Jan 26	*H*	36	0.52	3
Radio-Loud Quasars							
PKS 0258+011	1.221	20.5	2004 Nov 01	*H*	36	0.51	3
PKS 0432−148	1.899	21.2	2004 Oct 31	*K*	36	0.47	6
PKS 0442+02	1.430	20.5	2004 Nov 01	*K*	36	0.37	7
PKS 0511−220	1.296	19.5	2004 Nov 27	*H*	36	0.44	5
PKS 0805−07	1.837	19.8	2004 Dec 25	*K*	36	0.37	7
PKS 0837+035	1.570	20.7	2004 Dec 24	*K*	36	0.37	4
PKS 0845−051	1.242	19.4	2004 Dec 21	*H*	36	0.38	5
PKS 1015−31	1.346	20.4	2004 Dec 26	*H*	36	0.27	5
PKS 1046−222	1.609	21.7	2005 Jan 25	*K*	36	0.37	3

[a] Quasar *V*-band apparent magnitudes from Veron-Cetty & Veron (2003).
[b] Frame exposure time in minutes.
[c] The average FWHM of all stars in the frame in arcseconds.
[d] Number of stars used for the PSF modeling of each field.
[e] The 2QZ catalog contains two different redshift determinations for this object: $z_1 = 1.895$ and $z_2 = 1.343$. We adopt $z_1 = 1.895$ here because the 2QZ spectrum from which this value is inferred shows stronger emission lines.

$\sim 0.4''$ FWHM), of 17 quasars (10 radio-loud quasars [RLQ] and 7 radio-quiet quasars [RQQ]) in the redshift range $1 < z < 2$ to characterize their host galaxies. We found that the luminosity evolution of both RLQ and RQQ hosts until $z \sim 2$ is consistent with that of massive ellipticals undergoing passive evolution. There is no significant decrease in the host mass until $z \sim 2$, as would be expected in the models of hierarchical formation of massive ellipticals (Kauffmann & Haehnelt 2000). Note, however, that more recent hierarchical models, including, e.g., feedback due to AGNs and supernovae (e.g., Granato et al. 2004; Bower et al. 2006), are in agreement with the existence of a substantial population of massive ellipticals out to at least $z \sim 2$. We also found evidence that RLQ hosts are systematically more luminous (massive) by a factor ~ 2 than RQQ hosts at all redshifts. A similar result was obtained by Kukula et al. (2001) using a smaller sample of quasars at $z \sim 0.9$ and 1.9. Little correlation was found between the nuclear and the host luminosities. Note that at low redshift, some claims of a correlation between the two quantities have been reported in the literature (e.g., McLeod & Rieke 1994; Bahcall et al. 1997; Hooper et al. 1997), whereas some other studies of low-redshift quasars (e.g., Dunlop et al. 2003) have not found a correlation for high-luminosity quasars. Obviously, selection effects due to the difficulty of detecting faint galaxies hosting bright quasars, or vice versa, of detecting weak quasars located in bright host galaxies, may combine to form a spurious correlation (e.g., Hooper et al. 1997).

The majority of quasars studied at high redshift, including those in Falomo et al. (2004), belong to the bright end of the quasar luminosity function, due to the selection effects in flux-limited samples, e.g., the redshift-luminosity degeneracy. In this paper, we present an imaging study of a sample of lower luminosity quasars (by ~ 2 mag on average with respect to that of Falomo et al. 2004), to study the dependence of host properties on nuclear luminosity at high redshift. We therefore have a well-matched sample of quasars, and we are in a good position to study the significance of any correlation between the nuclear and the host luminosities. In § 2 we describe our sample, in § 3 we report the observations, and in § 4 we describe the data analysis. Our results for the observed quasars and their comparison with the host luminosities of quasars derived from other samples, the relationship between host and nuclear luminosities, and the cosmic evolution of RLQ and RQQ host galaxies are discussed in § 5. A summary of our results and directions for future work are given in § 6. We adopt the concordance cosmology with $H_0 = 70$ km s^{-1} Mpc^{-1}, $\Omega_m = 0.3$, and $\Omega_\Lambda = 0.7$.

2. THE SAMPLE

The sample of low-luminosity (LL) quasars was defined to match in redshift the sample of high-luminosity (HL) quasars of Falomo et al. (2004). It was extracted from the quasar catalog of Veron-Cetty & Veron (2003), requiring $1.0 < z < 2.0$, $M_V < -25.0$ at $z = 1.0$, increasing to $M_V < -26.3$ at $z = 2.0$, $-60^\circ < \delta < -8^\circ$, and having sufficiently bright stars within $1'$ of the quasar to allow a reliable characterization of the PSF. Our choice of a slightly redshift-dependent magnitude limit guarantees an optimal matching in redshift between the HL and LL subsamples, while roughly corresponding to a simple magnitude limit at $M_V \sim -25.8$. We included both RLQs and RQQs in order to investigate the difference between the host galaxies of the two types of quasars. Importantly, the LL and HL RLQ and RQQ subsamples are well matched in both their redshift and optical/blue luminosity distribution. This selection yielded in total 20 LL quasars, of which 15 quasars were imaged: nine RLQs and six RQQs (Table 1). There is no statistically significant difference in the properties of the original and the observed samples. Figure 1 shows the distribution of the observed quasars in the redshift-optical luminosity

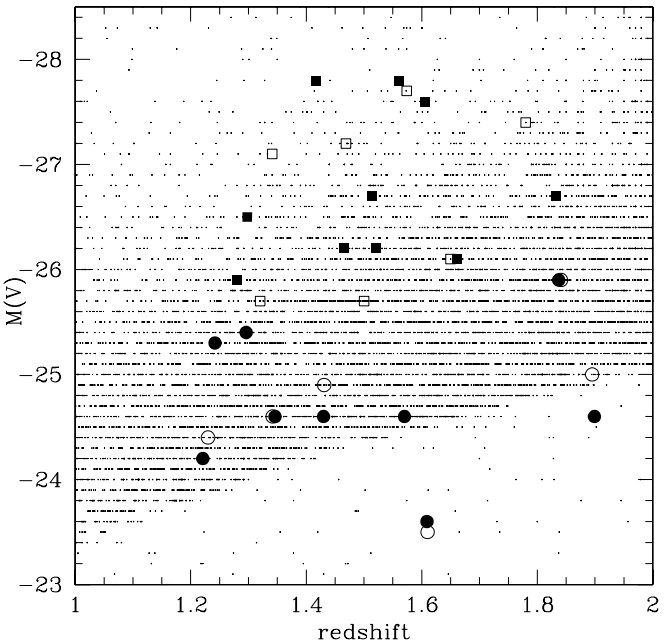

FIG. 1.—Distribution of the low-luminosity RLQs (*filled circles*) and RQQs (*open circles*) in the z-M_V plane, compared with the high-luminosity RLQs (*filled squares*) and RQQs (*open squares*) from Falomo et al. (2004), and for reference, with all quasars at $1 < z < 2$ in Veron-Cetty & Veron (2003; *small dots*).

plane compared to those for HL quasars in Falomo et al. (2004) and to all the quasars in Veron-Cetty & Veron (2003).

3. OBSERVATIONS

Deep images of the quasars in the H or K band were obtained using the near-infrared (NIR) ISAAC camera (Cuby et al. 2000), mounted on UT1 (Antu) of VLT at the European Southern Observatory (ESO) in Paranal, Chile. The short-wavelength (SW) arm of ISAAC is equipped with a 1024×1024 pixel Hawaii Rockwell array, with a pixel scale of $0.147''$ pixel^{-1}, giving a field of view of $\sim 150'' \times 150''$. The observations were performed in service mode in the period between 2004 October and 2005 January. A detailed journal of observations is given in Table 1. The seeing, as derived from the full width half maximum (FWHM) size of the image of stars in each frame, was consistently excellent during the observations, ranging from $\sim 0.3''$ to $\sim 0.5''$ (average and median FWHM $= 0.4''$). The choice of observing in the H and K band, for objects at below and above $z = 1.4$, respectively, was motivated by observing the same rest-frame wavelengths as a function of redshift.

Total integration times were 36 minutes per target. The images were secured using individual exposures of 2 minutes per frame, and a jitter procedure (Cuby et al. 2000), which produces a set of frames at randomly offset telescope positions within a box of $10'' \times 10''$, centered on the first pointing. Data reduction was performed by the ESO pipeline for jitter imaging data (Devillard 1999). Each frame was flat-fielded by a normalized flat field obtained by subtracting ON and OFF images of the illuminated dome, after interpolating over bad pixels. Sky subtraction was derived by median averaging sky frames from the 10 frames nearest in time. The reduced frames were aligned to subpixel accuracy using a fast object detection algorithm and co-added after removing spurious pixel values. Photometric calibration was performed using standard stars observed during the same night. The estimated internal photometric accuracy is ± 0.03 mag.

4. TWO-DIMENSIONAL DATA ANALYSIS

Two-dimensional data analysis has been carried out using AIDA, Astronomical Image Decomposition and Analysis (M. Uslenghi & R. Falomo 2007, in preparation), a software package specifically

TABLE 2
RESULTS OF THE RADIAL PROFILE MODELING

Quasar	z	Filter	$m_{\rm nucl}$[a]	$m_{\rm host}$[a]	r_e (arcsec)	χ^2_{dV}[b]	$\chi^2_{\rm exp}$[c]	$\chi^2_{\rm PSF}$[d]	dof[e]
Radio-Quiet Quasars									
Q0335−3546	1.841	K	17.9	20.1 ± 0.4	1.1 ± 0.5	0.6	0.4	1.4	8
MS 0824.2+0327	1.431	K	18.4	18.1 ± 0.1	0.5 ± 0.1	1.0	1.1	19.0	15
2QZ J101733−0049	1.342	H	19.0	20.2 ± 0.3	0.9 ± 0.2	1.3	1.2	4.2	12
2QZ J101733−0203	1.895	K	18.8	19.9 ± 0.2	1.0 ± 0.6	1.6	1.3	4.0	13
TOL 1033.1−27.3	1.610	K	19.2	17.3 ± 0.1	0.6 ± 0.1	3.6	1.5	67.1	35
Q1045+056	1.230	H	17.4	>20.1	...	...	...	0.9	11
Radio-Loud Quasars									
PKS 0258+011	1.221	H	17.5	19.0 ± 0.2	0.7 ± 0.2	0.8	1.0	6.6	23
PKS 0432−148	1.899	K	17.2	19.6 ± 0.3	1.2 ± 0.2	1.2	1.5	2.0	17
PKS 0442+02	1.430	K	16.5	16.8 ± 0.1	0.8 ± 0.2	1.1	3.5	33.5	39
PKS 0511−220	1.296	H	18.1	19.5 ± 0.3	0.7 ± 0.2	1.5	1.6	3.5	13
PKS 0805−07	1.837	K	16.0	>18.6	...	...	...	1.6	16
PKS 0837+035	1.570	K	17.6	19.3 ± 0.3	0.9 ± 0.3	1.0	2.4	4.1	10
PKS 0845−051	1.242	H	17.8	18.2 ± 0.1	0.6 ± 0.2	0.5	7.9	38.7	9
PKS 1015−31	1.346	H	16.1	18.1 ± 0.1	0.9 ± 0.2	1.0	2.3	17.7	26
PKS 1046−222	1.609	K	17.9	18.7 ± 0.2	0.7 ± 0.2	1.2	1.2	10.3	15

[a] Apparent magnitudes correspond to the indicated filter.
[b] The reduced χ^2 value of the fit with PSF and an elliptical host-galaxy model.
[c] The reduced χ^2 value of the fit with PSF and an exponential disk host-galaxy model.
[d] The reduced χ^2 value of the fit with only the PSF model. In the cases of Q1045+056 and PKS 0805−07, the χ^2 does not significantly improve when adding the galaxy component, therefore these objects are indicated as unresolved.
[e] Number of degrees of freedom.

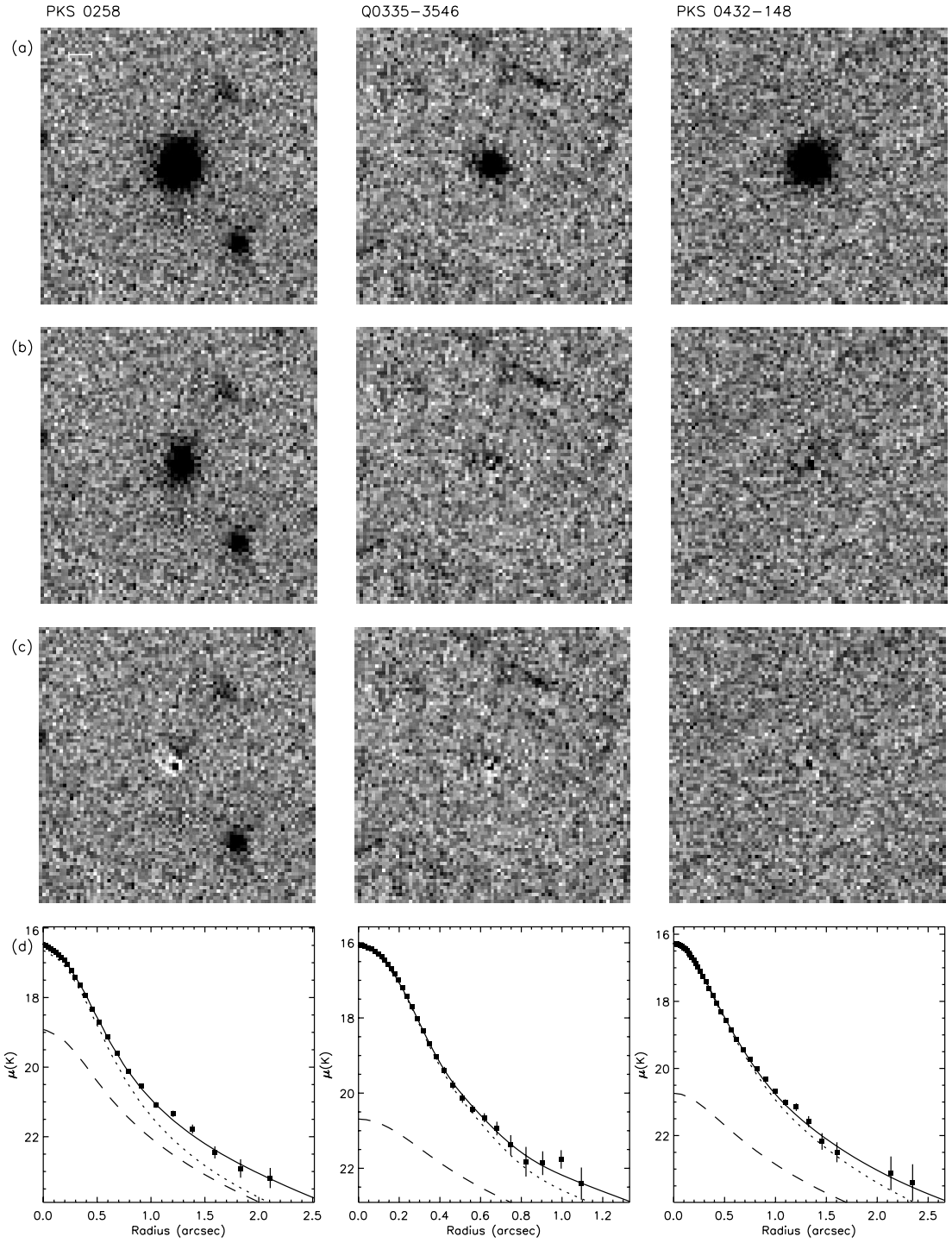

FIG. 2.—Images of the central $\sim 7'' \times 7''$ region surrounding the quasars, showing, from top to bottom, (*a*) the original image, (*b*) the image after subtracting a scaled PSF model (the host galaxy), and (*c*) the residuals. These panels are on a linear scale from $-3\ \sigma$ to $+3\ \sigma$, where σ is calculated from the sky noise. No interpolation, filtering, or smoothing is applied. Panel *d* shows the observed radial brightness profiles of the quasars (*filled squares*), superimposed to the fitted model consisting of the PSF (*dotted line*) and an elliptical (de Vaucouleurs law) galaxy convolved with its PSF (*dashed line*). The solid line shows the composite model fit.

designed to perform two-dimensional model fitting of quasar images, providing simultaneous decomposition into nuclear and host components. The analysis consists of two main parts: (1) PSF modeling and (2) quasar decomposition.

4.1. *PSF Modeling*

To detect the host galaxies of quasars and to characterize their properties, the key factors are the nucleus-to-host magnitude ratio and the seeing (the shape of the PSF). The most critical part of the analysis is thus to perform a detailed PSF modeling for each frame. This is based on fitting a parameterized bidimensional model to the field stars, which are selected based on FWHM, roundness, and signal-to-noise ratio. A sufficiently bright, saturated star was included in the list of reference stars in order to model the shape of the faint wing of the PSF, against which most of the signal from the surrounding nebulosity will be detected.

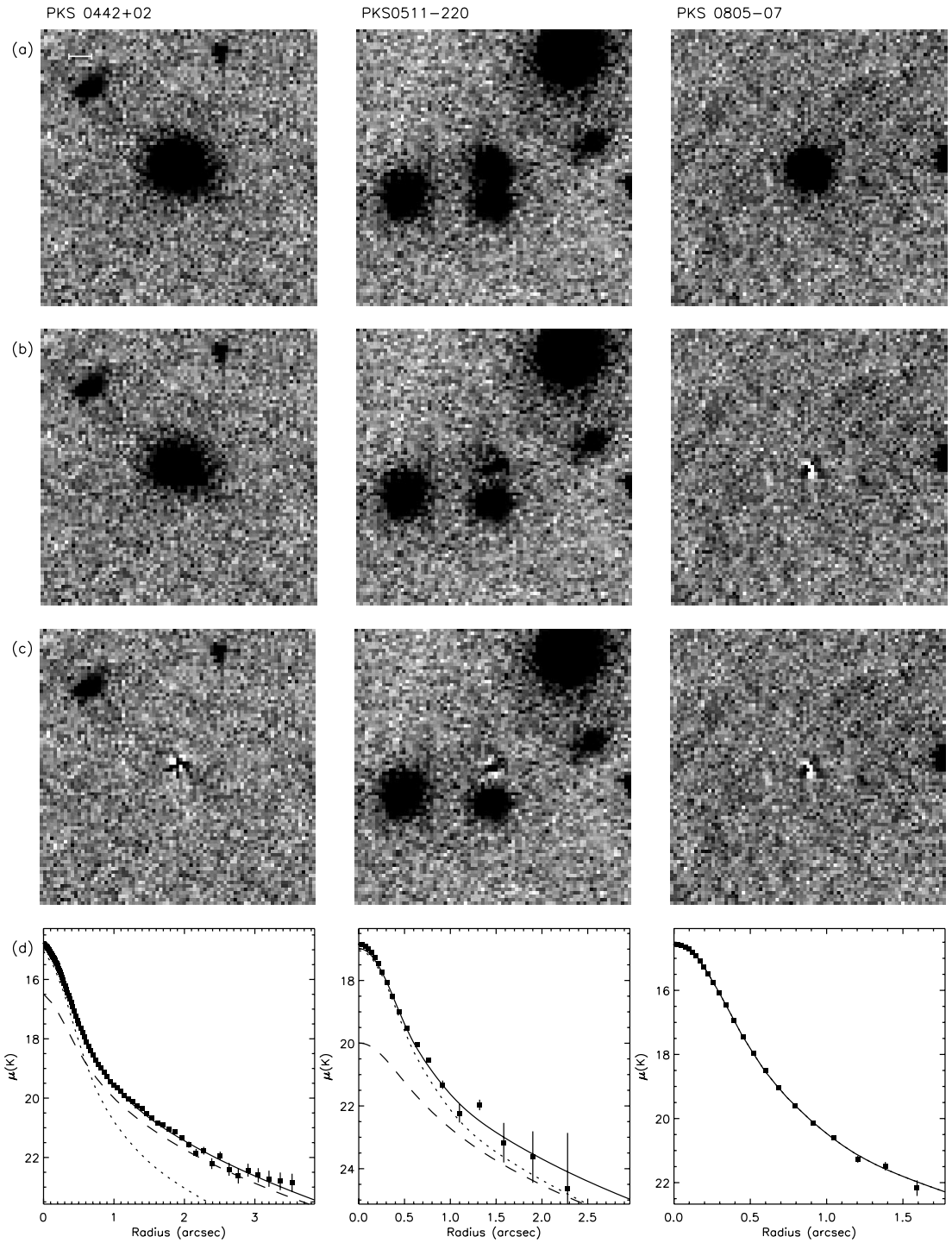

FIG. 2—*Continued*

The relatively large field of view of ISAAC (∼2.5′) and the constraint on the quasar selection to have at least one bright star within 1′ from the quasar allowed us to reach this goal and thus to perform a reliable characterization of the PSF. Images with a large number of stars distributed over the field of view have been checked to account for any possible positional dependence of the PSF. No significant variations were found, and in this analysis the PSF is assumed to be spatially invariant, i.e., the same model has been fitted simultaneously to all the reference stars of the image.

For each source, a mask was built to exclude contamination from nearby sources, bad pixels, and other defects affecting the image. The local background was computed in a circular annulus centered on the source, and its uncertainty was estimated from the standard deviation of the values computed in sectors of concentric subannuli included in this area. The region to be used in the fit was selected by defining an internal and an external radius of a circular area. Setting the internal radius to a nonzero value allows exclusion of the core of bright, saturated stars.

4.2. *Quasar Host Characterization*

Once a suitable model of the PSF was determined, the quasar images were first fitted with only the PSF model in order to

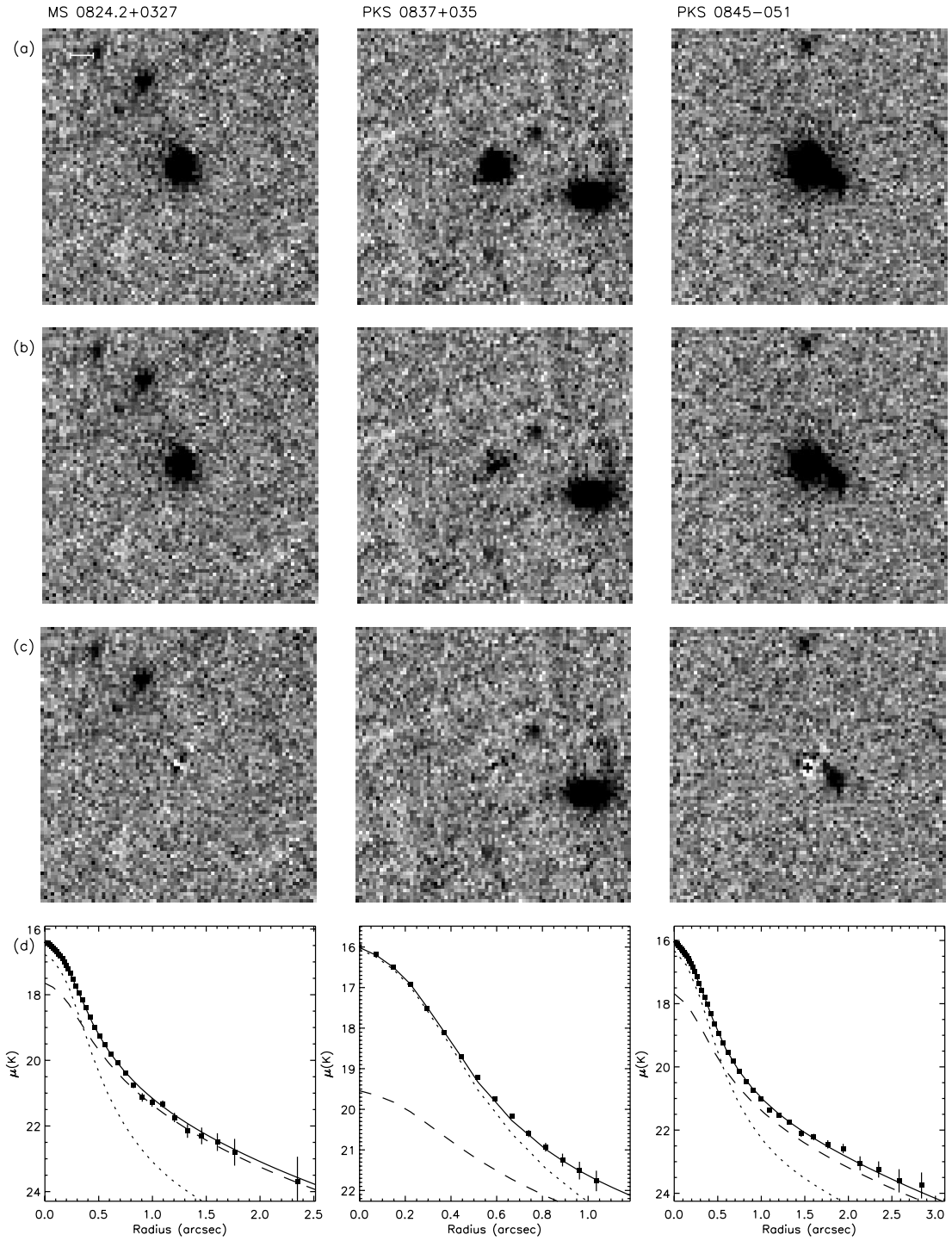

FIG. 2—*Continued*

provide a first indication of a deviation from the PSF shape. Then the object was fitted with a point source plus a galaxy modeled as a de Vaucouleurs $r^{1/4}$ or a disk model convolved with the PSF for the host galaxy, adding a scaled PSF to represent the nucleus. If the residuals did not reveal any significant deviation based on the comparison of the χ^2 values between PSF-only and PSF+host models, the object was considered unresolved.

With this procedure, we can derive the luminosity and the scale length of the host galaxies and the luminosity of the nuclei. An estimate of the errors associated with the computed parameters was obtained by simulating the process with synthetic data. Simulated quasar images were generated adding noise to the best-fit model, then the fit procedure was applied to these images, producing a "best-fit" combination of parameter values for each image. For each parameter, the standard deviation of the best-fit values gives an estimate of the uncertainty on the parameters. Obviously this procedure does not take into account systematic errors generated by imperfect modeling of the PSF, which can be roughly estimated by comparing results obtained with different PSF models, statistically consistent with the available data. In our worst case, Q0335−3546, for example, this effect produces an uncertainty of ∼0.3 mag on the brightness of the host galaxy.

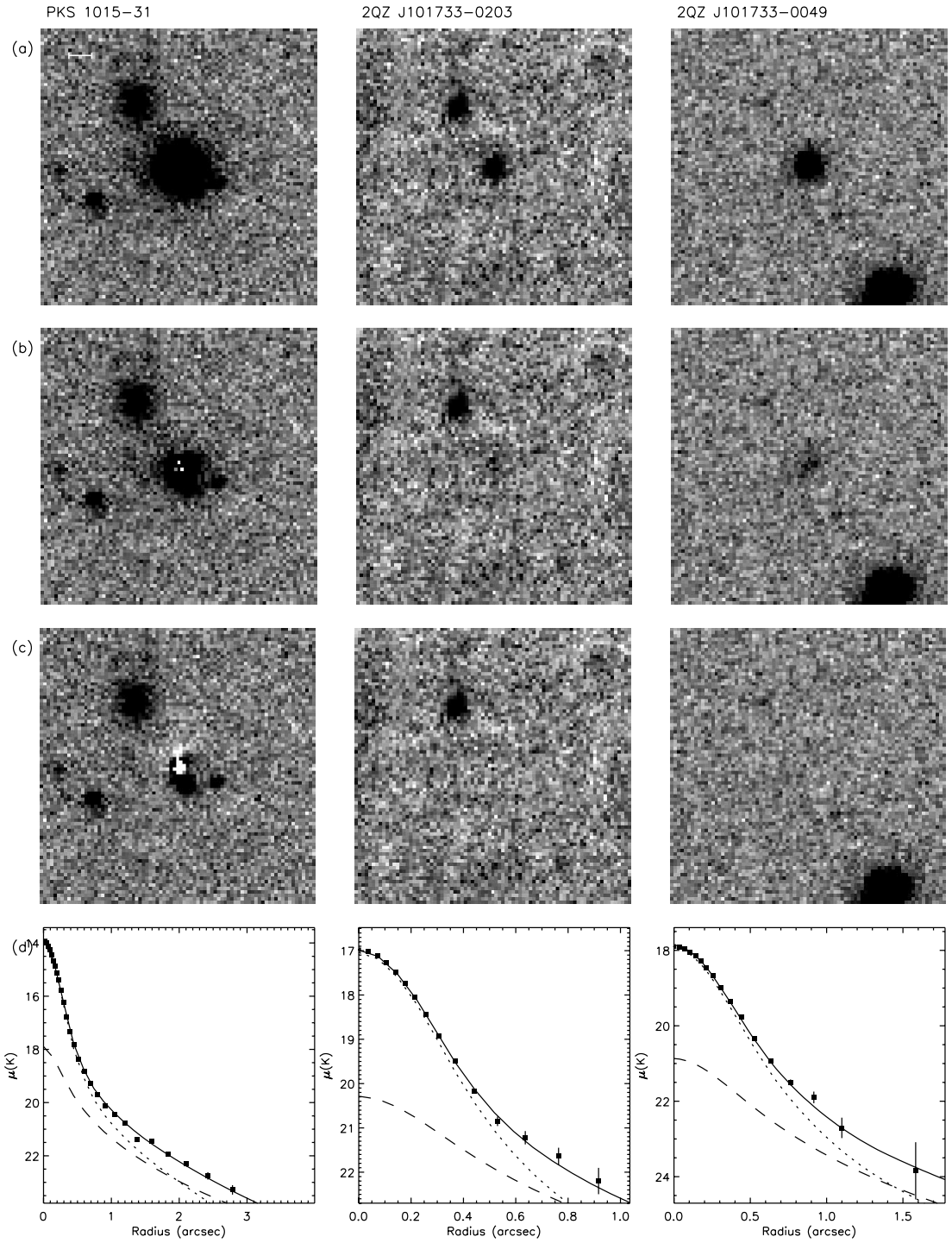

FIG. 2—*Continued*

Instead, in cases with a large number of suitable reference stars, the uncertainty is dominated by the noise. Upper limits to host magnitudes of unresolved objects were computed by adding a galaxy component to the PSF and varying its surface brightness until the model profile was no longer consistent with the observed profile.

While the total magnitude of the host galaxy can be derived with a typical internal error of 0.2–0.7 mag (0.4 mag on average), the scale length is often poorly constrained. This depends on the degeneracy that occurs between the effective radius r_e and the surface brightness μ_e (see Taylor et al. 1996).

At high redshifts it becomes difficult to distinguish between exponential disk and bulge models based on luminosity distributions. In this work, we have assumed that the host galaxies can be represented as elliptical galaxies following a de Vaucouleurs model. This is supported by the strong evidence at low redshift for the predominance of bulge-dominated hosts of quasars (e.g., Hamilton et al. 2002; Dunlop et al. 2003; Pagani et al. 2003 and references therein). Table 2 shows that for practically all the RLQs in our sample, we formally find a better fit (a lower χ^2 value) using a de Vaucouleurs model. For the RQQs, the situation is

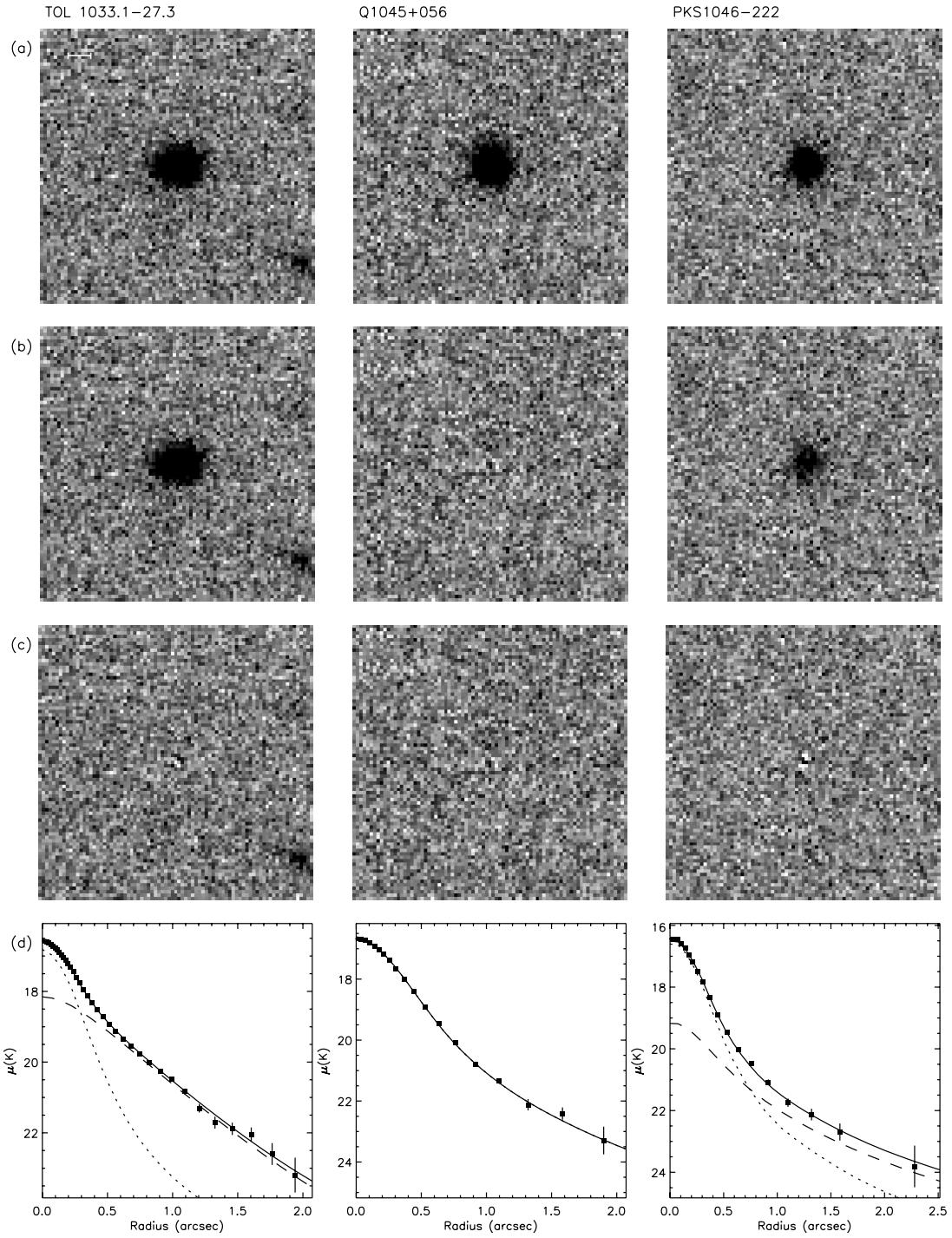

FIG. 2—*Continued*

reversed, with 4/5 objects formally having a better fit with a disk model. In most of these cases, however, the difference in the χ^2 value between the models is negligible. Note that adopting a disk model would result in fainter host galaxies by $\sim$0.5 mag on average, but this would not introduce systematic differences that would affect our conclusions.

5. RESULTS

In Figure 2, we report for each observed quasar the image of the quasar, the best-fitting host-galaxy model after subtracting a scaled PSF, the residuals after fitting the model, the radial brightness profile, and the best fit using the procedure described above. The parameters of the best fit, together with their estimated uncertainty, are given in Table 2. All quasars except two (RQQ Q1045+056 and RLQ PKS 0805−07) are resolved. This is quantified in Table 2 by comparing the reduced χ^2_ν value of the best fit including a host-galaxy model with that obtained from the best fit performed only with the PSF model.

In Table 3, we report the absolute magnitudes and the effective radii for each quasar host. As our observations in the redshift range $1 < z < 2$ were obtained in the *H* and *K* filters, the detections of the host galaxies roughly correspond to rest-frame

TABLE 3
PROPERTIES OF THE QUASARS AND THEIR HOST GALAXIES

Quasar	z	μ_e[a]	M_R(nucl)[b]	M_R(host)[b]	N/H[c]	$R_{\rm eff}$ (kpc)	M_U(tot)[d]
Radio-Quiet Quasars							
Q0335−3546	1.841	15.5	−24.9	−22.5	9.12	9.5	−26.0
MS 0824.2+0327	1.431	11.8	−23.7	−23.7	1.00	4.4	−25.1
2QZ J101733−0049	1.342	15.0	−23.6	−22.4	3.02	7.0	−24.7
2QZ J101733−0203	1.895	14.9	−24.1	−22.7	3.63	8.1	−25.2
TOL 1033.1−27.3	1.610	11.2	−23.2	−24.9	0.21	4.9	−23.9
Q1045+056	1.230	...	−25.2	>−22.3	>14.4	...	−24.5
Radio-Loud Quasars							
PKS 0258+011	1.221	13.1	−25.1	−23.3	5.25	5.3	−24.5
PKS 0432−148	1.899	15.0	−25.7	−23.1	11.0	9.7	−26.3
PKS 0442+02	1.430	11.5	−25.6	−25.0	1.74	6.9	−25.2
PKS 0511−220	1.296	13.7	−24.5	−23.0	3.98	5.5	−25.5
PKS 0805−07	1.837	...	−26.8	>−24.0	>13.2	...	−26.5
PKS 0837+035	1.570	14.3	−24.8	−22.8	6.31	7.8	−24.8
PKS 0845−051	1.242	12.2	−24.8	−24.2	1.74	5.0	−25.4
PKS 1015−31	1.346	12.8	−26.5	−24.5	6.31	7.2	−24.9
PKS 1046−222	1.609	13.1	−24.5	−23.5	2.51	6.2	−23.9

[a] Surface brightness (in mag arcsec^{-2}) at the effective radius, derived from the best-fit model.
[b] K-corrected absolute magnitudes of the nuclei and the host galaxies are reported in the R band; no correction for galactic extinction is applied.
[c] The N/H ratio refers to the absolute R magnitudes.
[d] The total U-band absolute magnitudes were calculated from the apparent V magnitudes in Veron-Cetty & Veron (2003) into our adopted cosmology and K-correction. The Galactic extinction was evaluated following Schlegel et al. (1998).

7000–8000 Å. This is also the case for the HL sample of Falomo et al. (2004). On the other hand, Kukula et al. (2001) and Ridgway et al. (2001) observed $z \sim 1.9$ quasars with the *HST* filter F165M, which corresponds to rest-frame 5500–6000 Å. Therefore, in order to refer all these observations to the same band (and to minimize the color and K-corrections), we transformed observed magnitudes into absolute magnitudes in the R band. Moreover, the use of R-band magnitudes offers the possibility of a relatively easy comparison with the majority of the published low-redshift quasar host studies. To perform the color and K-correction transformations, we assumed an elliptical galaxy template (Mannucci et al. 2001) for the host-galaxy magnitudes and a composite quasar spectrum (Francis et al. 1991) for the nuclear magnitudes. Note that the K-correction in the observed K band is almost independent of galaxy type up to $z \sim 2$, whereas in the observed H band at $1 < z < 1.5$, the K-correction depends on the assumed host-galaxy template, being ∼0.1–0.25 mag larger for elliptical galaxies than for spiral (Sc) galaxies (Mannucci et al. 2001).

5.1. *Properties of the Host Galaxies of Quasars at* $1 < z < 2$

In Figure 3, we compare the absolute R-band magnitudes of the quasar host galaxies versus redshift in this work, with the HL quasar hosts (Falomo et al. 2004), and with quasar hosts from Kukula et al. (2001) and Ridgway et al. (2001). Note that the $z \sim 2$ sample of Kukula et al. (2001) has on average a nuclear luminosity ($M_R = -24.9 \pm 0.9$) similar to our LL sample ($M_R = -24.9 \pm 1.0$), whereas the RQQs in Ridgway et al. (2001) at $z \sim 1.8$ are significantly fainter ($M_R = -23.3 \pm 1.2$). In order to treat these literature data homogeneously, we have considered the published apparent magnitudes in the H and K bands and transformed them to M_R, following our procedure (K-correction, cosmology and color correction). The average absolute R-band magnitudes of the host galaxies of the samples of LL RLQs and

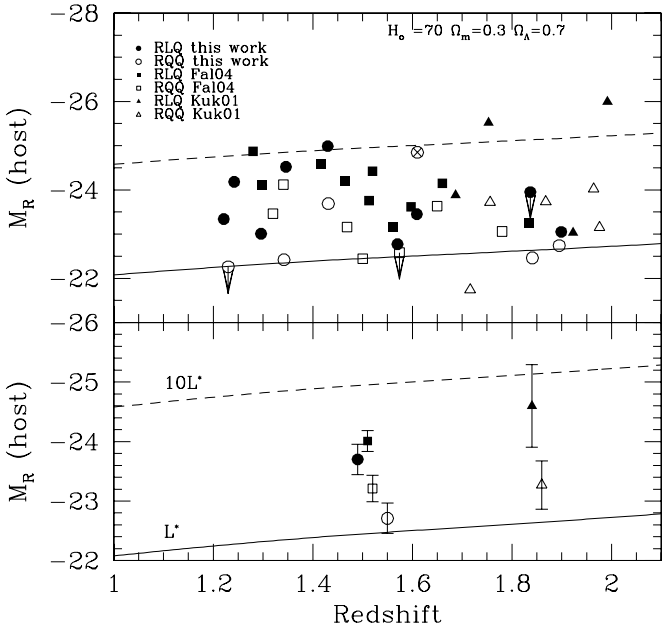

FIG. 3.—R-band absolute magnitude of the quasar host galaxies vs. redshift. The lines represent the expected behavior of a massive elliptical (at L^* and $10L^*$; *solid and dashed lines, respectively*) undergoing simple passive evolution (Bressan et al. 1994). For an explanation of the symbols, see Fig. 1. Also included are the RLQs (*filled triangles*) and RQQs (*open triangles*) from Kukula et al. (2001). The arrows represent the upper limits of the host luminosity for the unresolved objects Q1045+056, PHS 0805−07 (this work), and HE 0935−1001 (Falomo et al. 2004). The object marked with a cross is TOL 1033.1−27.3, for which our results indicate that a disk-galaxy model is a better fit to the data than a de Vaucouleurs law. Moreover, this object has by far the lowest N/H ratio in the sample and may in fact not host a quasar. The upper and lower panels show the data for individual quasars and for the sample averages, respectively.

TABLE 4
AVERAGE PROPERTIES OF THE QUASAR SAMPLES

Sample	Number	$\langle z \rangle$	$M(U)_{\rm nucl}$[a]	$M(R)_{\rm nucl}$	$M(R)_{\rm host}$	$(U-R)_{\rm nucl}$	References
HL RQQ	7	1.52 ± 0.16	-26.9 ± 0.9	-25.9 ± 1.0	-23.3 ± 0.6	0.80 ± 0.24	F04
HL RLQ	10	1.51 ± 0.16	-27.0 ± 0.7	-26.6 ± 0.9	-24.0 ± 0.6	0.37 ± 0.88	F04
LL RQQ	5[b]	1.55 ± 0.30	-25.1 ± 0.6	-24.1 ± 0.6	-22.8 ± 0.6	0.81 ± 0.86	This work
LL RLQ	9	1.49 ± 0.25	-25.2 ± 0.8	-25.2 ± 0.7	-23.7 ± 0.8	-0.16 ± 0.81	This work
RQQ	5	1.86 ± 0.12	-26.2 ± 0.2	-24.3 ± 0.5	-23.3 ± 0.9	1.94 ± 0.49	K01
RLQ	4	1.84 ± 0.14	-26.6 ± 0.2	-25.6 ± 0.5	-24.6 ± 1.4	0.93 ± 0.49	K01
RQQ	3	1.81 ± 0.07	-24.0 ± 0.3	-23.3 ± 1.2	-22.1 ± 0.7	0.68 ± 1.04	R01

[a] The calculated U-band luminosities have been K-corrected using the composite quasar SED, under the assumption that the underlying host galaxies make negligible contributions to the observed V-band magnitudes.
[b] The RQQ TOL 1033.1−27.3 (see the caption of Fig. 3) was excluded from the average.
REFERENCES.—(F04) Falomo et al. 2004; (K01) Kukula et al. 2001; (R01) Ridgway et al. 2001.

RQQs (this work) and HL RLQs and RQQs (Falomo et al. 2004) are given in Table 4.

Almost all the observed quasars have host galaxies with luminosities ranging between L^* and $10L^*$, where $M^*(R) \sim -21.2$ (Gardner et al. 1997; Nakamura et al. 2003) is the characteristic luminosity of the Schechter luminosity function for elliptical galaxies. For the LL quasars, there is a systematic difference in the luminosity between RLQ and RQQ host galaxies of $\sim$0.9 mag. A similar difference has been found in many previous studies of quasars at low redshift (Bahcall et al. 1997; Hamilton et al. 2002; Dunlop et al. 2003) and high redshift (Kukula et al. 2001). Floyd et al. (2004) found no difference between the RLQ and RQQ host luminosities at $z \sim 0.4$ [$\langle M_V \rangle$(RQQ) $= -23.35$, $\langle M_V \rangle$(RLQ) $= -23.07$ for elliptical host galaxies], but we note that their subsamples are not well matched in nuclear luminosity. The difference found in this work is also similar to that found for HL quasars ($\sim$0.7 mag; Falomo et al. 2004), and our new results thus confirm this offset, based on a larger statistical sample and a larger luminosity interval.

5.2. *The Relation between Nuclear and Host Luminosities*

If the mass of the central BH is proportional to the mass and thus to the luminosity of the spheroid of the host galaxy, as is observed for nearby inactive early-type galaxies (Kormendy & Richstone 1995; Magorrian et al. 1998), and if the quasar emits at a roughly fixed fraction of the Eddington luminosity, one would expect a correlation between the luminosity of the nucleus and that of the host galaxy. However, nuclear obscuration, beaming, and/or an intrinsic spread in the accretion rate and accretion-to-luminosity conversion efficiency could destroy this correlation.

Our combined sample of LL and HL quasars in this work and in Falomo et al. (2004) is designed to explore a large range of nuclear luminosity ($-23.5 < M_V < -28$; $H_0 = 50$ km s^{-1} Mpc^{-1}, $q_0 = 0$, corresponding to $-22.8 < M_V < -27.1$ in our adopted cosmology) and can therefore be used to investigate this issue. In Table 4, we report the average values of the rest frame U-band absolute magnitudes for the four subsamples (HL RLQ, LL RLQ, HL RQQ, and LL RQQ). These values are derived from the V-band apparent magnitudes reported in Veron-Cetty & Veron (2003), K-corrected and color corrected following the procedure described above. A correction for the Galactic extinction was applied following Schlegel et al. (1998).

Both in the LL and HL samples, the nuclear U-band luminosities of the RLQs and RQQs are matched within 0.1 mag. On the other hand, considering the rest-frame R-band nuclear luminosities, the RLQs appear more luminous than the RQQs by $\sim$1 mag. Note that also in the sample of Kukula et al. (2001), the quasars are well matched in the U band but not in the R band, where again the RLQs appear more luminous than the RQQs. These results, therefore, suggest that (at least in the redshift range considered here) there is a systematic color difference between the nuclei of RLQs and those of RQQs, in the sense that RLQs are redder than RQQs by $\sim$0.8 mag in the rest-frame $U - R$ color. Indeed, there is no apparent difference between the UV-to-NIR spectral properties of RLQs and RQQs in the well-known average quasar spectral energy distribution (SED) of Elvis et al. (1994), but the considered sample is biased toward X-ray and optically bright (i.e., bluer) quasars. Some hint of a possible difference between the SED of RLQs and RQQs was reported by Barkhouse & Hall (2001), who observed a greater NIR-to-optical luminosity ratio of RLQs with respect to RQQs in a large sample of quasars detected by 2MASS. Furthermore, Francis et al. (2000) found that the optical-NIR continuum is significantly redder in radio selected RLQs from the PKS Half-Jansky Flat-Spectrum Survey than in optically selected RQQs from the Large Bright Quasar Survey.

This effect may be interpreted as due to a differential extinction by dust or to an intrinsic difference of the strength of thermal and nonthermal emission components in the SEDs of RQQs and RLQs. For instance, in the case of flat-spectrum quasars, one could expect to observe an enhanced nonthermal (synchrotron) component contaminating the SED more in the near-IR than in the UV. Of course, this would suggest that the near-IR luminosity is not a good tracer of the bolometric emission. However, Francis et al. (2000) find that this effect is not sufficient to describe the spectral shape of all the sources in their radio-selected sample: about 50% of their PKS QSOs are more likely to be reddened by dust. We believe that with present data, both explanations (synchrotron contamination and dust extinction) are viable; however, in the specific case of our sample of RLQs, the hypothesis of synchrotron contamination is weakened because one third of the objects are steep-spectrum radio sources (viewed further away from the jet axis than flat-spectrum radio quasars) and there is no correlation between the radio spectral index and the $U - R$ (observed $V - K$) color. If extinction by dust is indeed the dominant effect, then the R band would be a better tracer of the bolometric luminosity than the U band. Moreover, we note that in the rest-frame U and B bands, the SED of a QSO is contaminated by the variable thermal emission in the accretion disk (the big blue bump), suggesting again that the R-band luminosity is a better indicator of the total nuclear emission.

In Figure 4, we compare the rest-frame R-band host and nuclear luminosities of the HL and LL quasars, together with quasars from Kukula et al. (2001) and Ridgway et al. (2001), both

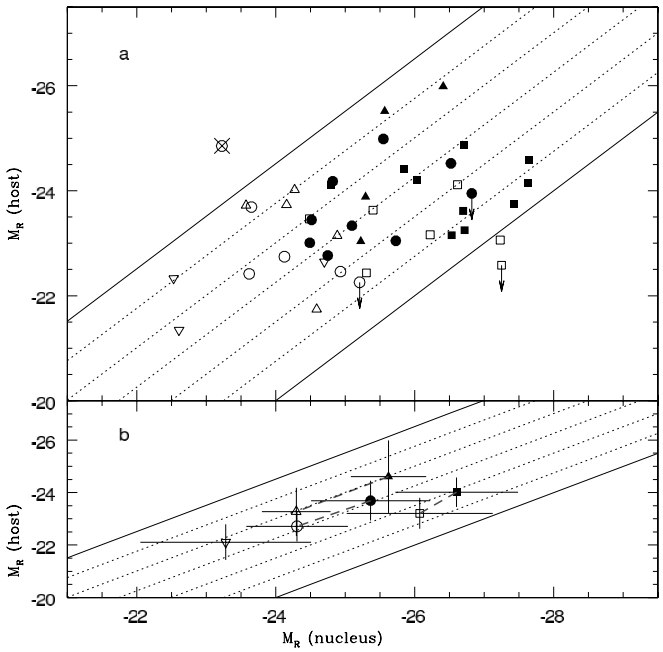

FIG. 4.—*Upper panel*: The absolute magnitude of the nucleus compared with that of the host galaxy. For an explanation of the symbols, see Figs. 1 and 3. Open inverted triangles are the RQQs from Ridgway et al. (2001). The arrows represent the upper limits of the host luminosity for the unresolved quasars Q1045+056, PKS 0805−07 (this work), and HE 0935−1001 (Falomo et al. 2004). The object marked with a cross is TOL 1033.1−27.3 (see the caption of Fig. 3). The diagonal lines represent the loci of constant ratio between host and nuclear emission. These can be translated into Eddington ratios, assuming that the central BH mass–galaxy luminosity correlation holds up to $z \sim 2$ and that the observed nuclear power is proportional to the bolometric emission. Separations between dotted lines correspond to a difference by a factor of 2 in the nucleus-to-host luminosity ratio. The two solid lines encompass a spread of 1.8 dex in this ratio. *Lower panel*: The average values for the seven subsamples considered here (see Table 4), excluding TOL 1033.1−27.3. Note that for each sample, the transition from RQQs to RLQs occurs at a roughly fixed fraction of the Eddington luminosity. [*See the electronic edition of the Journal for a color version of this figure*.]

for individual quasars (*upper panel*) and for the samples (*lower panel*). The resulting Spearman rank correlation coefficients (R_S), and the probabilities of obtaining the observed R_S values if no correlation is present are given in Table 5. Although this comparison is based on incomplete samples and is subject to uncertainties due to small number statistics, we find some correlation for the full sample of RLQs and RQQs [$R_S = 0.49$, and the probability of no correlation, $P(\mathrm{nc}) \sim 10^{-3}$]. This correlation becomes modest for RLQs [$R_S = 0.36$, $P(\mathrm{nc}) = 0.1$] and disappears altogether for RQQs [$R_S = 0.25$, $P(\mathrm{nc}) = 0.3$]. Generally, no such correlation has been found at low redshift (e.g., Dunlop et al. 2003; Pagani et al. 2003). However, interestingly, a trend similar to that found in this work is apparent from considering the data given in Hamilton et al. (2002), who studied a large sample of $z < 0.46$ quasars. We derived luminosities from their reported nuclear and host-galaxy apparent magnitudes, following our procedure, and we found a clear correlation for their full sample of quasars [$R_S = 0.56$, $P(\mathrm{nc}) = 10^{-3}$] and for their RLQs [$R_S = 0.51$, $P(\mathrm{nc}) = 10^{-2}$], while only a modest correlation is evident for their RQQs [$R_S = 0.38$, $P(\mathrm{nc}) = 0.1$]. This is an indication that the different trends of the nucleus-host luminosity relation displayed by RLQs and RQQs may be independent of redshift.

Assuming that the correlation between the central BH mass and the host-galaxy luminosity holds up to $z \sim 2$ and that the observed nuclear power is proportional to the bolometric luminosity, the observed nucleus-host luminosity correlation can be interpreted as the result of an intrinsically narrow distribution of the Eddington ratio. The observed scatter is then enhanced by the dispersion in the bulge luminosity–BH mass correlation and by intrinsic differences in the accretion rates. This is consistent with the relationship between the host galaxy and maximum nuclear luminosity observed at lower redshift (e.g., Floyd et al. 2004).

6. SUMMARY AND CONCLUSIONS

We have presented homogeneous high-resolution NIR images for a sample of 15 low-luminosity quasars in the redshift range $1 < z < 2$, to characterize the properties and the cosmological evolution of their host galaxies and to make a reliable comparison between RLQ and RQQ hosts. Together with the high-luminosity quasars previously studied by us, they cover a large range ($\sim$4 mag) of the quasar luminosity function.

The quasar host galaxies follow the trend in luminosity of massive inactive ellipticals (between L^* and $10L^*$) undergoing simple passive evolution. However, RLQ hosts appear systematically more luminous (massive) than RQQ hosts by a factor of $\sim$2. This difference is similar to that found for the high-luminosity quasars, and our new observations indicate that this gap is apparently independent of the nuclear luminosity in the observed V band (rest frame U band), in the sense that at a fixed observed B-band luminosity, the host galaxies of RLQs are a factor of $\sim$2 brighter in the observed H/K band (rest frame R band) than those of RQQs.

However, if the R-band nuclear luminosity is considered, the gap in the host luminosity could be ascribed to a difference in the total nuclear power. In fact (see Fig. 4), the magnitude gap of the host luminosity corresponds to a similar gap in the nuclear R-band luminosity, suggesting that at a fixed host mass (and BH mass), the same bolometric power is emitted.

For the combined sample of RQQs and RLQs, we find some correlation between the nuclear and the host luminosities, albeit with a large scatter, possibly due to a varying accretion efficiency. If the host luminosity is proportional to the black hole mass, quasars emit in a narrow range of power with respect to their Eddington luminosity. This range does not depend on redshift or on the radio properties of the quasars.

TABLE 5

THE SPEARMAN RANK CORRELATION COEFFICIENTS FOR M_R(NUCL) VERSUS M_R(HOST) IN THE QUASAR SAMPLES

	RQQ			RLQ			(RQQ + RLQ)		
SAMPLE	Number[a]	R_S	$P(\mathrm{nc})$[b]	Number[a]	R_S	$P(\mathrm{nc})$[b]	Number[a]	R_S	$P(\mathrm{nc})$[b]
HL + LL	12	0.33	0.3	19	0.38	0.1	31	0.44	10^{-2}
All samples	20	0.25	0.3	23	0.36	0.1	43	0.49	10^{-3}

[a] Number of objects in the considered subsample.
[b] Probability of no correlation, i.e., probability of obtaining the observed R_S values if no correlation is present.

Determining the quasar host properties at even higher redshift, around the peak epoch of quasar activity ($z \sim 2.5$) and beyond, requires very high S/N observations with a very narrow reliable PSF. We have an on-going program to tackle this problem using NIR adaptive optics imaging with NACO on VLT for high-luminosity quasars (Falomo et al. 2005, 2007), and NIR nonadaptive optics with ISAAC on VLT for low-luminosity quasars (J. Kotilainen et al. 2007, in preparation). Color information for the hosts (e.g., deep *R*-band imaging to target rest-frame UV emission), spectroscopy to estimate the BH masses of high-redshift quasars, and the study of environments as a function of redshift and radio power, will also be addressed in future work.

This work was partially supported by the Italian Ministry for University and Research (MIUR) under COFIN 2002/27145, ASI-IR 115 and ASI-IR 35, ASI-IR 73, and by the Academy of Finland (projects 8201017 and 8107775). This publication makes use of data products from the Two Micron All Sky Survey, which is a joint project of the University of Massachusetts and the Infrared Processing and Analysis Center, California Institute of Technology, funded by the National Aeronautics and Space Administration and the National Science Foundation. This research has made use of the NASA/IPAC Extragalactic Database (NED), which is operated by the Jet Propulsion Laboratory, California Institute of Technology, under contract with the National Aeronautics and Space Administration.

REFERENCES

Bahcall, J. N., Kirhakos, S., Saxe, D. H., & Schneider, D. P. 1997, ApJ, 479, 642
Barger, A. J., et al. 2001, AJ, 122, 2177
Barkhouse, W. A., & Hall, P. B. 2001, AJ, 121, 2843
Barth, A. J. 2004, in IAU Symp. 222, The Interplay among Black Holes, Stars, and ISM in Galactic Nuclei, ed. T. Storchi-Bergmann, L. C. Ho, & H. R. Schmitt (Cambridge: Cambridge Univ. Press), 3
Bettoni, D., Falomo, R., Fasano, G., & Govoni, F. 2003, A&A, 399, 869
Bower, R. G., et al. 2006, MNRAS, 370, 645
Boyle, B. J. 2001, Advanced Lectures on the Starburst-AGN Connection, ed. I. Aretxaga, D. Kunth, & R. Mujica (Singapore: World Scientific), 325
Bressan, A., Chiosi, C., & Fagotto, F. 1994, ApJS, 94, 63
Chary, R., & Elbaz, D. 2001, ApJ, 556, 562
Cuby, J. G., Lidman, C., Moutou, C., & Petr, M. 2000, Proc. SPIE, 4008, 1036
Devillard, N. 1999, in ASP Conf. Ser. 172, Astronomical Data Analysis Software and Systems VIII, ed. D. M. Mehringer, R. L. Plante, & D. A. Roberts (San Francisco: ASP), 333
Dunlop, J. S., & Peacock, J. A. 1990, MNRAS, 247, 19
Dunlop, J. S., et al. 2003, MNRAS, 340, 1095
Elvis, M., et al. 1994, ApJS, 95, 1
Falomo, R., Carangelo, N., & Treves, A. 2003, MNRAS, 343, 505
Falomo, R., Kotilainen, J. K., Pagani, C., Scarpa, R., & Treves, A. 2004, ApJ, 604, 495
Falomo, R., Kotilainen, J. K., Scarpa, R., & Treves, A. 2005, A&A, 434, 469
———. 2007, A&A, submitted
Ferrarese, L. 2006, Joint Evolution of Black Holes and Galaxies, ed. M. Colpi et al. (New York: Taylor & Francis), 1
Ferrarese, L., & Merritt, D. 2000, ApJ, 539, L9
Floyd, D. J. E., et al. 2004, MNRAS, 355, 196
Franceschini, A., Hasinger, G., Miyaji, T., & Malquori, D. 1999, MNRAS, 310, L5
Francis, P. J., Whiting, M. T., & Webster, R. L. 2000, Publ. Astron. Soc. Australia, 17, 56
Francis, P. J., et al. 1991, ApJ, 373, 465
Gardner, J. P., Sharples, R. M., Frenk, C. S., & Carrasco, B. E. 1997, ApJ, 480, L99
Gebhardt, K., et al. 2000, ApJ, 539, L13
Granato, G. L., De Zotti, G., Silva, L., Bressan, A., & Danese, L. 2004, ApJ, 600, 580
Hamilton, T. S., Casertano, S., & Turnshek, D. A. 2002, ApJ, 576, 61
Häring, N., & Rix, H. W. 2004, ApJ, 604, L89
Hooper, E. J., Impey, C. D., & Foltz, C. B. 1997, ApJ, 480, L95
Hunt, L. K., et al. 1997, ApJS, 108, 229
Kauffmann, G., & Haehnelt, M. 2000, MNRAS, 311, 576
Kauffmann, G., et al. 2003, MNRAS, 346, 1055
Kormendy, J., & Richstone, D. 1995, ARA&A, 33, 581
Kotilainen, J. K., & Ward, M. J. 1994, MNRAS, 266, 953
Kukula, M. J., et al. 2001, MNRAS, 326, 1533
Madau, P., Pozzetti, L., & Dickinson, M. 1998, ApJ, 498, 106
Magorrian, J., et al. 1998, AJ, 115, 2285
Mannucci, F., et al. 2001, MNRAS, 326, 745
Marconi, A., & Hunt, L. K. 2003, ApJ, 589, L21
Marconi, A., et al. 2004, MNRAS, 351, 169
McLeod, K. K., & Rieke, G. H. 1994, ApJ, 431, 137
McLure, R. J., & Dunlop, J. S. 2002, MNRAS, 331, 795
Nakamura, O., et al. 2003, AJ, 125, 1682
Pagani, C., Falomo, R., & Treves, A. 2003, ApJ, 596, 830
Percival, W. J., Miller, L., McLure, R. J., & Dunlop, J. S. 2001, MNRAS, 322, 843
Ridgway, S., Heckman, T., Calzetti, D., & Lehnert, M. 2001, ApJ, 550, 122
Schlegel, D. J., Finkbeiner, D. P., & Davis, M. 1998, ApJ, 500, 525
Steidel, C. C., Adelberger, K. L., Giavalisco, M., Dickinson, M., & Pettini, M. 1999, ApJ, 519, 1
Taylor, G. L., Dunlop, J. S., Hughes, D. H., & Robson, E. I. 1996, MNRAS, 283, 930
Veron-Cetty, M. P., & Veron, P. 2003, A&A, 412, 399
Warren, S. J., Hewett, P. C., & Osmer, P. S. 1994, ApJ, 421, 412
Yu, Q., & Tremaine, S. 2002, MNRAS, 335, 965